Materials Today • Volume xxx, Number xx • xxxx 2022 RESEARCH

RESEARCH: Original Research

Facile fabrication of 2D material multilayers and vdW heterostructures with multimodal microscopy and AFM characterization

Siyan Dong [1,2], Xiang Zhang [3], S. Shiva. P. Nathamgari [1,2], Andrey Krayev [4], Xu Zhang [1,2], Jin Wook Hwang [1,2], Pulickel M. Ajayan [3], Horacio D. Espinosa [1,2,*]

[1] Department of Mechanical Engineering, Northwestern University, Evanston, IL 60208, United States
[2] Theoretical and Applied Mechanics Program, Northwestern University, Evanston, IL 60208, United States
[3] Department of Materials Science and NanoEngineering, Rice University, Houston, TX 77005, United States
[4] Horiba Scientific, Novato, CA 94949, United States

Reliable transfer processes that enable manipulation of two-dimensional (2D) materials, e.g., transition metal dichalcogenides (TMDCs) and MXenes, from one substrate to another has been a necessity for successful device fabrication. With both mechanical exfoliation and chemical vapor deposition (CVD) widely used, a versatile, clean, deterministic, and yet simple transfer technique is highly needed. To address such need, we developed a transfer method that takes advantage of wettability contrast between interfaces without the use of sacrificial layers or chemical processes. More importantly, a setup was developed to carry out this transfer method with high sample selectivity and fine control of the position and orientation of transferred TMDC crystals, a feature required for fabrication of the devices based on vertical 2D heterostructures. Using both exfoliated and CVD grown materials and subsequent atomic force microscopy (AFM), photoluminescence (PL), confocal Raman and tip enhanced Raman spectroscopy (TERS) characterization, we ascertained the quality of interfaces resulting from the transfer process while preserving excellent 2D material integrity. PL and TERS maps revealed nanometer-scale heterogeneities in the interfaces of fabricated heterostructures, which should enable further perfection of the transfer technique. TERS/TEPL information were employed to identify areas suitable for nanodevice fabrication, making the reported transfer and characterization methods ideal for making high quality assembly of 2D heterostructure more accessible, which should facilitate exploration of vertical 2D heterostructures for applications in electronics, batteries, solar cells, and twistronics.

Keywords: 2D materials; 2D material transfer; Van der Waals heterostructure; Tip-enhanced Raman spectroscopy

Two-dimensional (2D) crystals have gone through a decade of emerging interests and rapid discovery [1,2]. When they transition from the bulk to monolayer form, different 2D materials—such as graphene (semimetal) and transition metal dichalcogenides (TMDCs, semiconductors), exhibit various unique properties: superior electron mobility and Young's modulus in graphene [3,4], intrinsic direct band-gap in MoS_2 [5], and piezoelectricity in monolayer TMDCs due to absence of an inversion symmetry center [6]. Many of these unique properties arise on account of quantum confinement and surface effects as the bulk material is reduced to few-layers and down to the monolayer limit. This provides an unprecedented palette of new materials

* Corresponding author.
E-mail address: Espinosa, H.D. (espinosa@northwestern.edu)

 https://doi.org/10.1016/j.mattod.2022.01.002

Please cite this article in press as: S. Dong et al., Materials Today (2022), https://doi.org/10.1016/j.mattod.2022.01.002

of relevance to applications in energy, electronics, and sensors. Indeed, the potential capabilities of 2D materials have been demonstrated in transistors, sensors, ferromagnets and resonators with a variety of device configurations [7–13]. The many-body complexes inherent in 2D materials and the endless possibilities to enhance and tune their properties have spurred in-depth theoretical and experimental studies to take advantages of different classes of 2D materials toward advanced electronic and optoelectronic device performance, including exploring the flexibility in the 3rd dimension with heterostructures [14–16]. Notably, in the semiconductors community, TMDCs such as MoS_2 and WS_2 are believed to be ideal candidates for next generation electronics to meet the demand associated to Moore's law [17,18].

Emerging high-volume applications call for reliable fabrication methods with high efficiency and controllability. The first steps of every device fabrication effort inevitably involve the preparation and transfer of a 2D material flake. There have been extensive reports on methods to produce monolayer 2D materials using mechanical exfoliation and chemical vapor deposition methods [1,19,20], as well as reports on the transfer of 2D materials with varying levels of complexity and tradeoffs. Depending on the device application, the growth (or exfoliation) substrate may not be the final foundation for the 2D material in the final configuration; hence, the process of transferring 2D material flakes to a different substrate remains an indispensable step in most device fabrications. A transfer process is also important when a device requires pick-and-place of a 2D material flake onto a prepared chip with pre-patterned structures. In addition, the transfer of 2D materials is a critical step for prototyping 2D heterostructures, where the layer-by-layer assembly from monolayers of the same/different materials is the priority [21]. One of the most commonly reported method is the polymethyl methacrylate (PMMA) film based wet transfer [22], which makes use of a spin-coated PMMA film as the transfer medium and a sacrificial layer, usually SiO_2 or a water soluble layer such as aqua-SAVE® [23]. After dissolving the sacrificial layer, the 2D flakes carried by the PMMA can be "scooped" up by the target substrate. However, residue-free removal of PMMA layer is hard to obtain, and the scooping operation makes placement precision and wrinkle-free transfer challenging [24]. Another common method makes use of polydimethylsiloxane (PDMS) as a stamp. Exfoliated 2D material flakes on Nitto tape are transferred to PDMS first and then the PDMS serving as a stamp is positioned and adhered to the target substrate. After peeling off, the 2D flakes are transferred to the target substrate [25]. This is a robust process, which can be done with a very basic setup. However, with increasing use of CVD grown specimens for scalability and throughput, transfer processes require more versatility to deal with both mechanically exfoliated and CVD grown flakes, as the CVD grown 2D materials are commonly prepared on a rigid substrate and cannot be efficiently peeled onto tapes or PDMS through a mechanical exfoliation process. Other effective transfer methods have been developed such as using Elvacite as a sacrificial layer and employing water soluble polymers as a mediator [26,27]. These methods nevertheless involve usage of sacrificial layers, which present some complexities, e.g., removal of sacrificial layers can require harsh environment, and complete removal of sacrificial layers can be challenging as residues are usually found on 2D material flakes afterwards [28–30]. Many attempts have been made to achieve cleaner and easier transfer using capillary force to pull 2D flakes from substrates [31,32], exploiting water to weaken 2D materials-substrate interaction for easier pick-up [33–37], adopting water soluble salt sacrificial wafers [38], and making use of thermal release tapes as stamps [39]. Despite this progress, there is still need for development of a simple, clean, and precise transfer mechanism with augmented versatility to enable exploration of 2D heterostructures made from CVD-grown as well as mechanically exfoliated flakes. We note that the CVD method can produce single, bi- and tri-layers of TMDCs, e.g., of MoS_2, with controlled recipes, but the process does not provide orientation control between layers [40,41].

In this work, we report a new method that utilizes mismatch of water wettability of different contact surfaces to achieve efficient, clean, and precise 2D material transfer using PDMS-stamps, and a microscopy setup for flake alignment. In a parallel effort, the mismatch in water wettability mechanism was utilized by Lee et al. to achieve high quality graphene transfer from an Al_2O_3 substrate [42]. Here, we show that the method is capable of addressing both mechanically exfoliated and CVD grown TMDC monolayers with high yield, and more importantly, the fine spatial and orientation placement control for heterostructure assembly, all with ease of operation and without the usage of sacrificial layers or harsh chemical environments. By conducting Raman, photoluminescence, tip-enhanced Raman spectroscopy (TERS), and high-resolution transmission electron microscopy (HRTEM), we demonstrate that the transfer method can selectively assemble high-quality 2D crystal heterostructures with precise control of location, micrometer level precision, and registration angle. We also reveal heterogeneities in assembled 2D heterostructures through tip-enhanced methods to shed light on device design considerations. The methodology is expected to impact the emerging fields of heterostructure devices and twistronics [43].

Results and discussion

The transfer method presented here makes use of the competing surface energies between different interfaces to control the direction of transfer. Such mechanism echoes the process of temporary tattoo transfer that people enjoy during holidays and festivities. During a tattoo transfer process, water is applied after application onto human skin to weaken the interaction between the ink-film and the backing paper. This ensures that the ink-film favors the skin and stays after peeling off the backing paper [44]. The basic form of the transfer process is illustrated in Fig. 1. Starting with TMDC flakes on a Si/SiO_2 substrate, a PDMS stamp is first brought into contact. The assembly is then immersed in 75 °C deionized water before the stamp is peeled off from the substrate, carrying the TMDC flakes with it. After drying, this PDMS stamp can be stamped onto a target substrate, and with the assistance of mild heating (60–80 °C) it is subsequently peeled off to achieve transfer of the TMDC flakes from Si/SiO_2 to the target substrate. Note that during the transfer process only the PDMS stamp and water are used, and no chemical etching is involved.

Please cite this article in press as: S. Dong et al., Materials Today (2022), https://doi.org/10.1016/j.mattod.2022.01.002

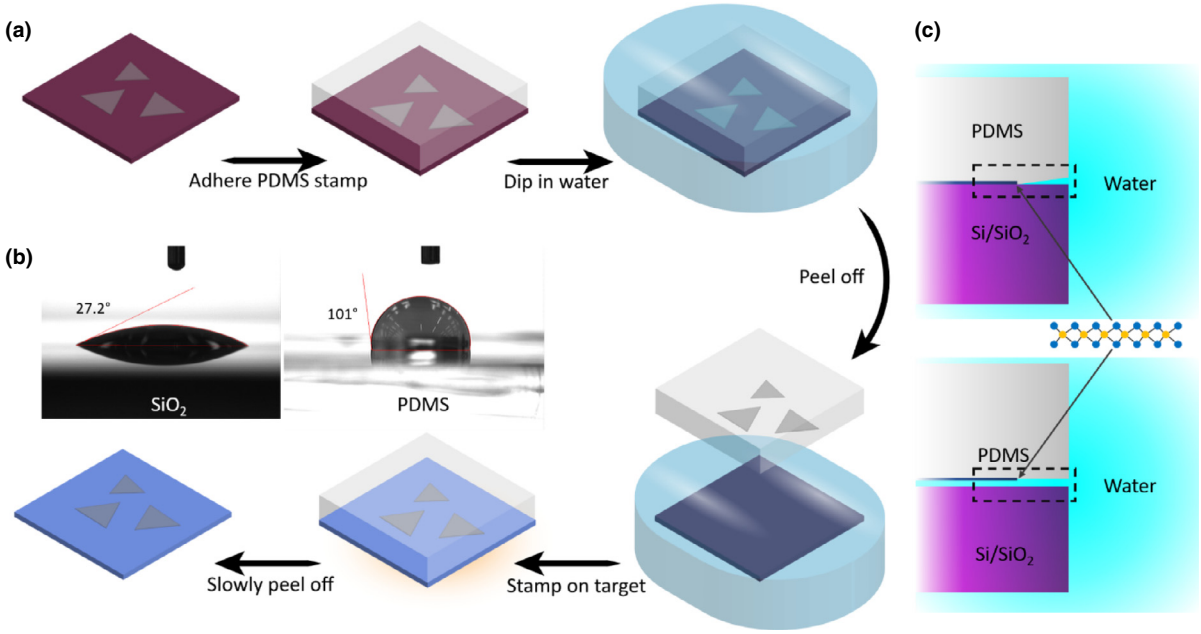

FIGURE 1

Schematic illustration of the transfer process. (a) TMDC flakes prepared on Si/SiO_2 substrate are picked up by a PDMS stamp assisted by selective weakening of interfaces using water. The stamp carrying TMDC flakes is then pressed onto the target substrate. Slow peeling of the PDMS stamp completes the transfer process. (b) Contact angle measurements on SiO_2 and untreated PDMS substrates, respectively. (c) Utilization of the competing interface energies is initiated by water penetration through the PDMS-Si/SiO_2 contact. Then, as water is met by PDMS-2D flake-Si/SiO_2 interface, it favors wetting the 2D flake-Si/SiO_2 interface due to higher hydrophilicity, thus "cleaving" through the 2D flake-Si/SiO_2 contact.

Mechanically exfoliated and CVD grown TMDCs are commonly prepared on a thermally grown SiO_2/Si substrate, which is a hydrophilic surface when clean [45]. Likewise, freshly prepared TMDCs such as MoS_2 possess good surface wettability (~50 mJ/m^2) [46]. The key to the flake removal from the substrate is to take advantage of the difference in wettability between the PDMS stamp and the SiO_2 surface. When a PDMS stamp is brought into contact with 2D TMDC flakes prepared on SiO_2, a PDMS-TMDCs-SiO_2 "sandwich" is formed, involving two interfaces: PDMS-TMDCs and TMDCs-SiO_2. At the beginning of this process, water is first met with an interface between PDMS and SiO_2, where a split-injection flow pattern initiates selective water penetration [47]. The hydrophilic-hydrophobic contrast between untreated PDMS and SiO_2 drives water to penetrate this gap favoring wetting the TMDCs-SiO_2 interface, thus selectively separating the TMDCs-SiO_2 contact and allowing TMDC flakes to adhere to the PDMS stamp (analogous to how water weakens interaction between tattoo ink and backing paper to allow pattern transfer). This separation mechanism can be estimated by comparison of surface energies before and after separation of TMDCs and SiO_2, which expose the two surfaces to water. The change in surface energy can be expressed as $\Delta\gamma = \gamma_{TMDC\text{-}S} - \gamma_{S\text{-}W} - \gamma_{TMDC\text{-}W}$, where $\gamma_{TMDC\text{-}S}$ is the adhesion energy between TMDC flakes and SiO_2, $\gamma_{S\text{-}W}$ is the interfacial tension between SiO_2 and water, and $\gamma_{TMDC\text{-}W}$ is the interfacial tension between TMDC flakes and water. Applying Young's equation yields

$$\Delta\gamma = \gamma_{TMDC-S} - \gamma_{TMDC} - \gamma_S + \gamma_W(cos\theta_{TMDC} - cos\theta_s) \quad (1)$$

where γ_{TMDC} is the surface energy of TMDC flakes, γ_T is the surface energy of SiO_2, and γ_T surface tension of water. To use MoS_2 as an example, the adhesion energy $\gamma_{TMDC\text{-}S}$ has been reported to be 170 mJ/m^2 [48]. Using typical measurements of surface energies of SiO_2 (~200 mJ/m^2), MoS_2 (~50 mJ/m^2) and water (~72 mJ/m^2) [45,46], it can be shown that $\Delta\gamma < 0$, making water-driven separation of TMDC-SiO_2 more energetically favorable. Contact angle measurements in Fig. 1b verified the contrasting wettability on SiO_2 and PDMS drives the transfer. This TMDCs-SiO_2 interface weakening also manifests itself in the experimental observation that simple water immersion without agitation serves to remove a portion of TMDC flakes on a SiO_2 substrate. During transfer to the target substrate, the viscoelasticity of the PDMS stamp, which "flows" overtime as it is being peeled very slowly, plays an important role. In this context, heating at 80 °C during the final stamping process promotes better adhesion between the 2D materials and target substrate surface. Importantly, the process described here can be finished in a few minutes without the need of a ventilated hood. According to Eq. (1), the same exact pick-and-place protocol is expected to work for graphene since (1) its adhesion energy to SiO_2 is comparable to that of MoS_2 and (2) the surface energy of graphene is higher (which would make the picking of graphene from SiO_2 more favorable) [49,50]. The stamping transfer step is governed by the release of the carrier PDMS, so most target substrates with an atomically smooth surface are expected to be suitable target substrates.

Fig. 2 shows a simple demonstration of this transfer method using freshly mechanically exfoliated MoS_2. Optical images at different steps of the transfer process were recorded for verification. Fig. 2a–c show an area of interest containing a monolayer MoS_2 on the original Si/SiO_2 substrate after exfoliation, subse-

Please cite this article in press as: S. Dong et al., Materials Today (2022), https://doi.org/10.1016/j.mattod.2022.01.002

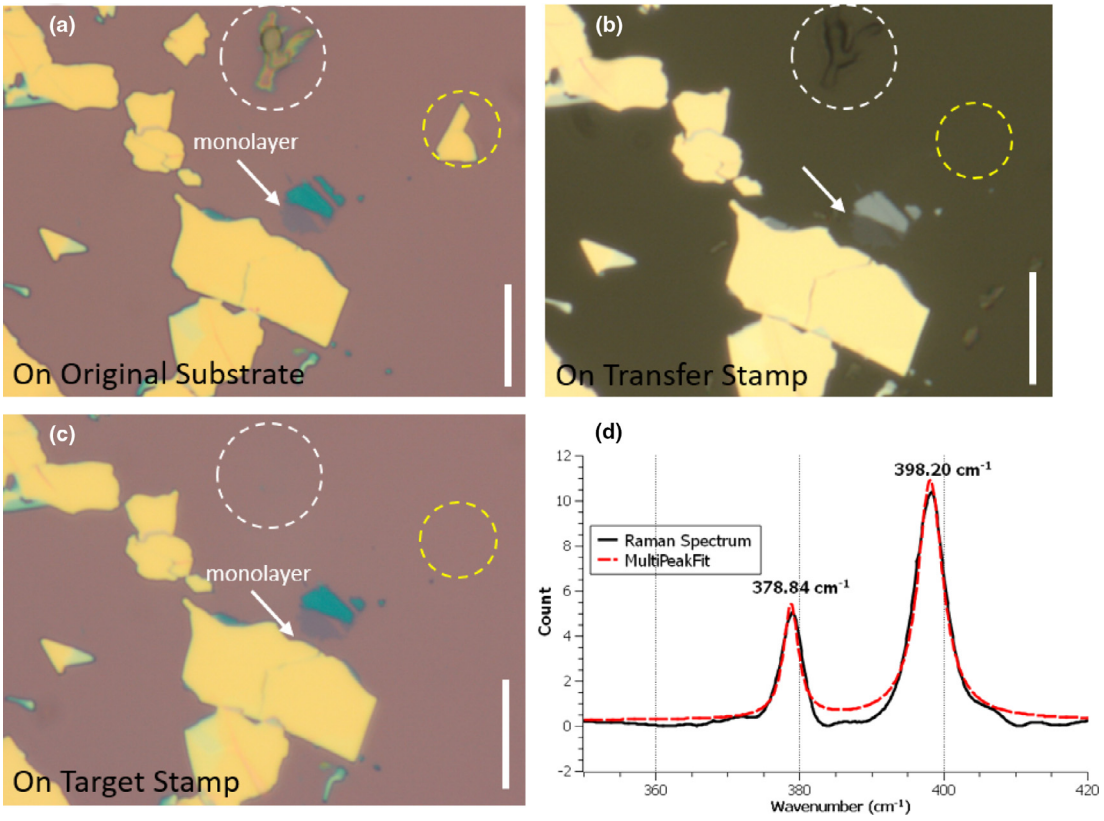

FIGURE 2

Demonstration of successful transfer of mechanically exfoliated MoS_2. (a–c) MoS_2 flake of interest on original SiO_2 substrate, PDMS and target SiO_2 substrate, respectively. (d) Raman spectrum acquired post-transfer shows high sample quality. (Scale bars: 10 μm).

quently being picked up on the PDMS gel stamp, and finally transferred to target pristine SiO_2 substrate, respectively. The images taken at different stages of the transfer process are compared side by side. Through comparison of total MoS_2 flakes area before and after the transfer (Fig. 2a vs 2c), a yield of 92% is estimated, as the flakes annotated by yellow circles are the only loss during transfer, possibly due to poorer local contact with the PDMS stamp. Additionally, an add-on advantage is the removal of a piece of residual adhesive from the tape used for mechanical exfoliation (compare white circles in insets a and c). This is a convenient feature as residual adhesives can disrupt subsequent fabrication steps (such as causing unwanted comets in spin coating and poor lift-off after deposition), affecting quality of final devices. Raman spectroscopy was used to further attest the quality of the transferred MoS_2 flakes. Two peaks between 350 cm^{-1} and 450 cm^{-1} were found, corresponding to the E^1_{2g} and A_{1g}.

Raman modes of monolayer MoS_2 with a peak separation of 19.35 cm^{-1} was determined by curve fitting. This indicates the structural integrity is well preserved after the transfer procedure and the material was not doped by polymer residue [51]. To further validate the mechanism of this transfer method, trial pick-up experiments were performed with the following control conditions: no water added, use of IPA instead of water, and use of water but without heating. Absence of water and substitution of water with IPA both yielded essentially no effective pick-up of TMDC flakes from the SiO_2. In the absence of heating, the pick-up process worked only with low yield. This is due to local variations of surface energy terms in Eq. (1) may result in $\Delta\gamma > 0$ for some flakes. Warm water with lower γ_W term helps to ensure $\Delta\gamma < 0$ and facilitate water penetration for successful transfers. Results of this comparison are consistent with the transfer mechanism and can help guide the development of the operation protocol.

As a further step, it is possible to implement this transfer in a controllable, *in-situ* manner to allow positioning, aligning, and selectivity due to the absence of sacrificial layers and wet processes in this method. A setup, illustrated in Fig. 3, was developed consisting of a glass slide mounted on a 3-axis micromanipulator, a bottom stage with translation and rotation capabilities, a custom-built, thin, silicone hot plate, and an optical microscope for visualization. An SU-8 mold was fabricated to make PDMS stamps (Fig. 3b) with mini protrusions. These protrusions make it possible to select the stamp's contact location and selectively pick up TMDC flakes of interest locally. The smaller contact area also allows much more uniform contact to improve pick-up and stamping consistency. The SU-8 mold was designed with different protrusion sizes (50–500 μm in lateral lengths) and different shapes (circular and rectangular) to accommodate various sizes of area of interest. This enabled us to pick up the flakes of interest with minimum impact on the surrounding areas. Herein, we do not examine the transfer of larger continuous monolayer flakes since we aim at precise alignment of the crystalline orientations of the 2D monolayer flakes. The transfer of larger flakes would require larger PDMS stamps and more importantly, good

Please cite this article in press as: S. Dong et al., Materials Today (2022), https://doi.org/10.1016/j.mattod.2022.01.002

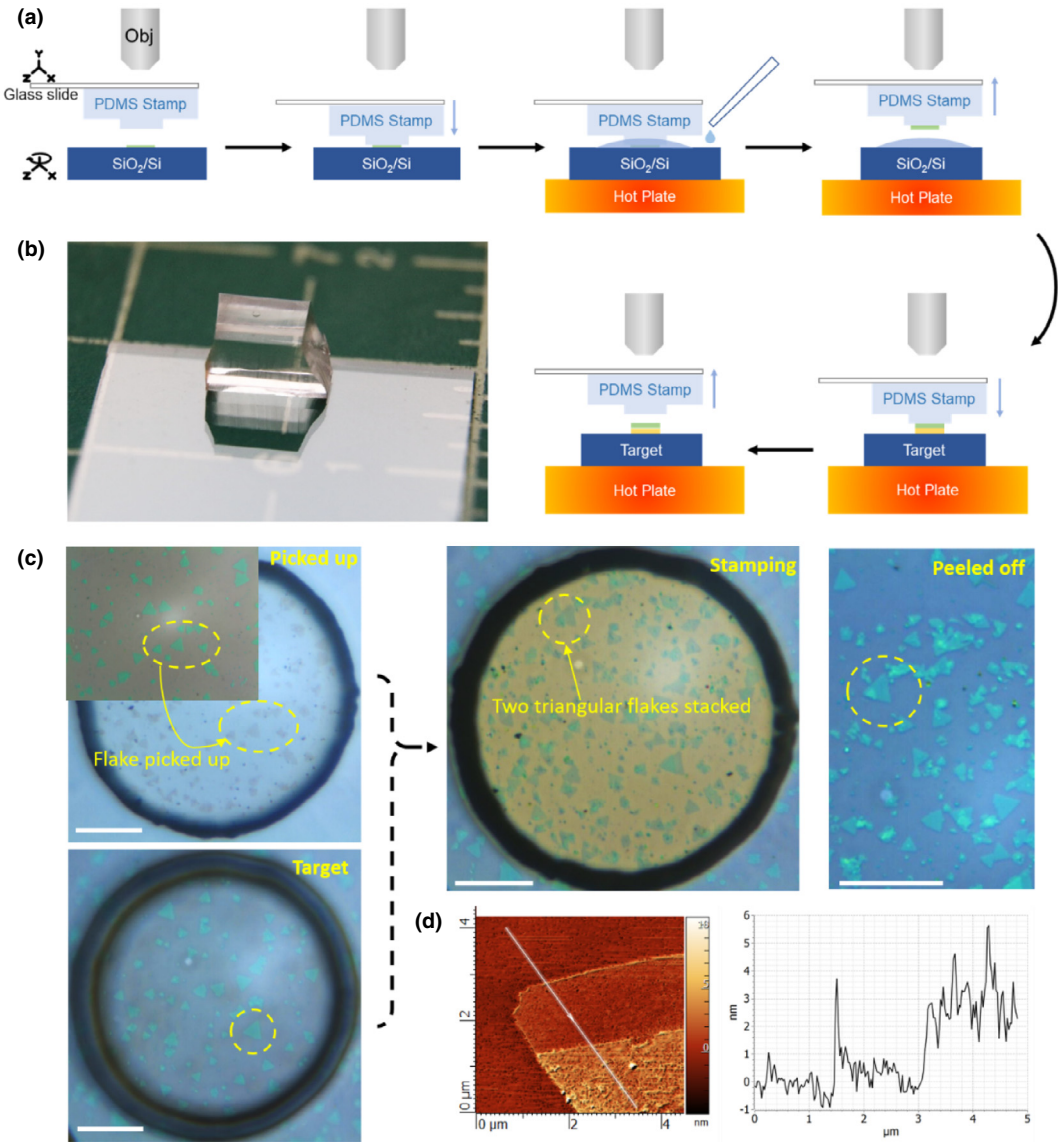

FIGURE 3

(a) Steps for deterministic transfer. Pre-fabricated PDMS stamp with small rectangular extrusion is adhered to a glass slide and aligned to 2D materials of interest for pick-up. Then water is added around the interface to allow penetration and separation. After picking up the bottom is swapped with the target substrate and the picked up 2D material can be precisely positioned and transferred to any location on the target substrate. (b) Macro photograph of a PDMS stamp fabricated from a SU-8 mold, which allows batches of stamps of different dimensions to be prepared in each run. (Obj = Objective). (c) Demonstration of the PDMS stamp selective transfer process. CVD $MoSe_2$ flakes were identified and picked up by the PDMS stamp with a circular protrusion area. Through the transparent stamp, the surface of the target substrate was brought into focus to identify and position flakes with desired orientation. Then the stamp was brought into contact with the target substrate. Using a slow peeling rate, all the flakes on the stamp were transferred to the target substrate and no changes of flake geometry or fractures were observed. Scale bars: 50 µm. (d) AFM topography reveals perfect alignment accuracy and confirms 2D material steps assembled by the reported process. Bubbles and spikes were visible, and they formed due to contact with the PDMS stamp and air during the pick-up and stamping process, which introduced trapped air bubbles or uncured PDMS.

quality flakes with flaw sizes within the critical length. The latter is governed by the synthesis process. After achieving contact at the protruded surface using the micromanipulator, a pipette is used to dispense deionized water to the area of contact in place of the original water bath. Heating with the silicone hot plate to 75 °C assists faster water penetration into the material interfaces to "wedge" into the space between the substrate and the 2D materials. This was supported by a study by Desai et al. [52], which shows that elevated temperature facilitates water spreading with higher surface energy on SiO_2. We note that a lower temperature may be desirable for preserving sensitive materials. An oxygen plasma treatment on the entire PDMS, except the protruding regions, which are masked with tape, was also found to assist water penetration. The rate of water intercalation was not intentionally controlled, a feature that can be investigated by changing process parameters. The stamp moves up with the materials picked up, the original substrate is removed, the stamp is dried using nitrogen gun, and the target substrate is placed under the PDMS stamp. By employing the optical microscope imaging and 3-axis micromanipulator stage

Please cite this article in press as: S. Dong et al., Materials Today (2022), https://doi.org/10.1016/j.mattod.2022.01.002

with rotation, one can locate and determine where to "drop" the picked up TMDC flake. Finally, the transfer is achieved by approaching the stamp to the aligned location and retracting slowly. The peeling process is carefully controlled manually through the z-motion of the stamp-carrying stage so that the meniscus of retracting contact between the PDMS and the target substrate moves at approximately 5 μm/s or lower. Through multiple tests we found that the stamp transfer efficiency was not very sensitive to meniscus retracting rate as long as it does not quickly propagate in an uncontrolled manner. The PDMS stamps can be reused by simply drying (if not contaminated by debris) or oxygen plasma cleaning (if contaminated) followed by air exposure for several days to restore the hydrophobicity of the surface.

The method here presented can assemble bilayer to multilayer 2D heterostructures with accurate control of spatial alignment and relative angle between layers. The anisotropic nature of monolayer TMDC properties makes vertical assembly of 2D heterostructure nontrivial as varying alignment of crystal orientation may produce remarkably different device properties. Even though the stacking orientation dependent properties of 2D heterostructure crystals is out of the scope of this work, we do strive to provide a reliable method to enable such efforts. The molded PDMS stamps allow picking up of a small area of TMDC samples. As demonstrated in Fig. 3c, a selected area of CVD grown $MoSe_2$ prepared on SiO_2 substrate was successfully picked up by a circular PDMS stamp micro-protrusion. The optically transparent stamp was then positioned over the target substrate where features on the target substrate were visible. Alignment between the flakes on the stamp and the desired "landing zone" on the target substrate was achieved for 2D materials stacking where two $MoSe_2$ triangles were assembled with the same orientation. Since this whole process was performed under a probe station microscope, all steps were closely monitored for high controllability. The precision of the spatial positioning is limited by the resolution of the imaging system, precision of stages, and minute drifting during stamp contact due to PDMS deformation. Using stages with micrometers, we recorded a lateral positioning precision better than 1 μm. The theoretical accuracy of the angle alignment is about ±1.15 degrees, given a typical length of 100 pixels for a TMDC flake in our imaging system and a ±2 pixels in resolving the edge of the flake. In reality, non-ideal manual operation and minor setup drift exist and will affect the accuracy. Atomic Force Microscopy (AFM) topography at the site of 2D flakes stacking revealed that almost perfect alignment between two stacked 2D material flakes was achieved, indicated by the overlapping straight edges of the two triangular flakes (Fig. 3d). The assembled sample surface was free of sizable contamination. In the current setup, only the area of the protruding stamp contributes to the transfer process, meaning the rest of the target substrate area remains intact and is preserved for future experiments, leading to efficient utilization of 2D material. Additionally, since the transfer principle applies to both exfoliated and CVD grown TMDC flakes, one can stack combination of TMDC flakes from different preparation methods with fine position and rotation control. We compared the method herein to several existing transfer techniques with an emphasis on the potential limitations of those methods that are mitigated herein, as shown in Table 1.

TABLE 1

Comparison between the method adopted herein and previously reported techniques.

Work	Method	Aspects that could be improved	Improvements implemented herein
Dean et al.[22] Chen et al.[29]	PMMA carrier film with chemical etching	Chemical etching needed. Process requires longer time and the operator's skills	Only water is involved in the material release step, which happens in a few minutes
Zhu et al.[23] Li et al.[37] Van Ngoc et al.[30]	PMMA carrier film without etching	No fine control of material placement	Fully controllable and accurate pick-up and stamp-down process
Castallanos-Gomez et al.[25]	Direct transfer with Gelfilm®	Only demonstrated for mechanically exfoliated materials that are transferred to the stamp from a tape	Works with both exfoliated and CVD grown materials prepared on a substrate
Lu et al.[26]	Water soluble mediator	No fine control of material placement	Fully controllable and accurate pick-up and stamp-down process
Zomer et al.[27]	Polymer carrier with glass holder	Requires removal of the polymer carrier film	Clean process without further chemical treatment
Uwanno et al.[28]	Fully dry PMMA transfer	Selective transfer of a small region is not feasible	Flexibility in selecting specific areas
Ma et al.[31] Hou et al.[32]	Capillary-force-assisted transfer	No fine control of material placement in an *in situ* manner	Fully controllable and accurate pick-up and stamp-down process; flexibility in controlling area sizes
Jin et al. [34] Kim et al.[33] Gurarslan et al[36].	Surface energy assisted transfer	Requires sophisticated operation to pick up floating 2D materials/carrier films.	Fully controlled and monitored steps
Han et al. [38]	Water-dissoluble salt wafer	Salt wafer constrains the type of materials that can be transferred	Good versatility for various types of 2D materials grown on SiO_2
Kang et al.[39]	Thermal release tape pick-up and transfer	Focus on large layer sizes and potentially high volume stacking; limited selectivity of pick-up and placement control	Focuses on developing "small volume" device fabrication with higher pick-up and placement flexibility

Please cite this article in press as: S. Dong et al., Materials Today (2022), https://doi.org/10.1016/j.mattod.2022.01.002

In order to verify the composition and atomic level material integrity, we used HRTEM to inspect the assembled heterostructures. A stacked MoS_2-on-$MoSe_2$ heterostructure and a MoS_2-on-MoS2 bilayer, prepared using the protocol described above, were characterized. HRTEM images shown in Fig. 4 reveal that the lattice structures were preserved with very few vacancies. Moiré patterns reveal misalignment angles of 8.5° and 13.5° for the assembled $MoS_2/MoSe_2$ heterostructure and the MoS_2/MoS_2 bilayer, respectively. The material composition for the $MoS_2/MoSe_2$ heterostructure is confirmed by Energy Dispersive Spectroscopy (EDS) with the atomic % ratio of Mo:S:Se ~1:1:1. For the assembled MoS_2 bilayer, the atomic % ratio is Mo:S ~1:1.9.

To characterize the quality of assembled heterostructures, Raman and photoluminescence (PL) spectroscopy were used. Here, we present representative cases with a 2D structure consisting of CVD grown $MoSe_2$ triangles (CVD $MoSe_2$/CVD $MoSe_2$, Heterostructure 1) and a 2D heterostructure formed by CVD grown $MoSe_2$ and mechanically exfoliated MoS_2 (CVD $MoSe_2$/exfoliated MoS_2, Heterostructure 2). In Fig. 5, the two assembled 2D heterostructures are demonstrated. For Heterostructure 1, two CVD $MoSe_2$ triangles were assembled with parallel edges. Raman spectroscopy obtained right after completion of the transfer process (Fig. 5b) shows the A_{1g} peak, corresponding to out-of-plane mode, at approximately 239 cm^{-1}, consistent with the presence of monolayer $MoSe_2$ [53]. This indicates the two individual monolayer triangles were stacked with weak interactions, acting as separate monolayers. This result was not unexpected. 2D materials are very sensitive to surface contaminations, e.g., polymeric residues, and water molecules can easily get trapped between the two layers [54,55]. After annealing in vacuum at 200 °C for 2 h, the Raman spectrum obtained at the same location with the same acquisition parameters showed the A_{1g} peak red shifted by about 1 cm^{-1}, while the A_{1g} location remained unchanged on the monolayer region. The shift in A_{1g} peak is consistent with previous reports, corresponding to bilayer $MoSe_2$, where the existence of interlayer interaction redshifts the A_{1g} mode frequency [53,56]. This strongly suggests that the annealing process served to successfully remove interlayer contaminants and improve adhesion. Due to the transition from an indirect bandgap to a direct bandgap from bulk to monolayer, strong photoluminescence emissions are expected from monolayer $MoSe_2$ flakes. This was confirmed right after assembly of Heterostructure 1, where the stacked $MoSe_2$ flakes behaved like monolayers. After annealing (Fig. 5c), the PL peak energy close to 810 nm remained unchanged, indicating the band structure was not altered by the transfer process. An apparent PL quenching of this peak was identified, which was consistent with existing reports on stacked CVD heterostructures, suggesting more efficient charge transfer across layers [57].

Fig. 5d–f shows Heterostructure 2 consisting of a CVD grown $MoSe_2$ flake transferred onto an exfoliated MoS_2 flake. Different heterostructures were formed simultaneously when the monolayer CVD $MoSe_2$ triangle overlapped with both a monolayer and a bilayer tip of the exfoliated MoS_2 flake, making an approximate 90° edge-edge angle with the bilayer portion. With Raman spectroscopy, we probed both the 1L $MoSe_2$/1L MoS_2 and the 1L $MoSe_2$/2L MoS_2 regions after annealing. The same A_{1g} mode peak at 239 cm^{-1} was identified on both spectra, consistent with monolayer-like response of $MoSe_2$ in both cases. Near the 400 cm^{-1} wavenumber, peak pairs with separations of 19 cm^{-1} and 22 cm^{-1} were observed, which correspond to characteristics of A_{1g} and E^1_{2g} modes of monolayer and bilayer MoS_2, respectively [58]. CVD $MoSe_2$ and exfoliated MoS_2 both retained their own Raman fingerprints as they were stacked into heterostructures, which was expected as their different lattice constants prevent interlayer Raman mode coupling. In photoluminescence spectra acquired from both 1L $MoSe_2$/1L MoS_2 and 1L $MoSe_2$/2L MoS_2 regions, the $MoSe_2$ PL emission peak at 790 nm was distinguished

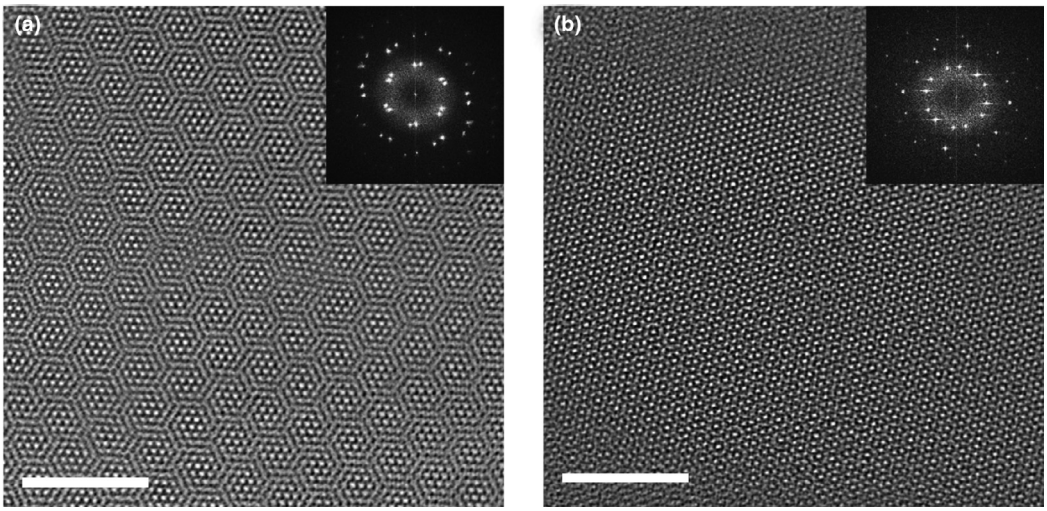

FIGURE 4

(a) HRTEM image of a $MoS_2/MoSe_2$ heterostructure transferred to a holey TEM grid using the method herein reported. The Moiré pattern corresponds to a misalignment angle of 8.5°, as measured from the FFT image (inset). EDS confirms that the bilayer is MoS_2 and $MoSe_2$ with an atomic % ratio of Mo:S:Se ~ 1:1:1. (b) HRTEM image of a MoS_2/MoS_2 assembled bilayer transferred to a holey TEM grid using the method herein reported. The Moiré pattern corresponds to a misalignment angle of 13.5°, as measured from the FFT image (inset). EDS confirms that the bilayer is MoS_2 with an atomic % ratio of Mo:S: ~ 1:1.9. Scale bars: 5 nm.

Please cite this article in press as: S. Dong et al., Materials Today (2022), https://doi.org/10.1016/j.mattod.2022.01.002

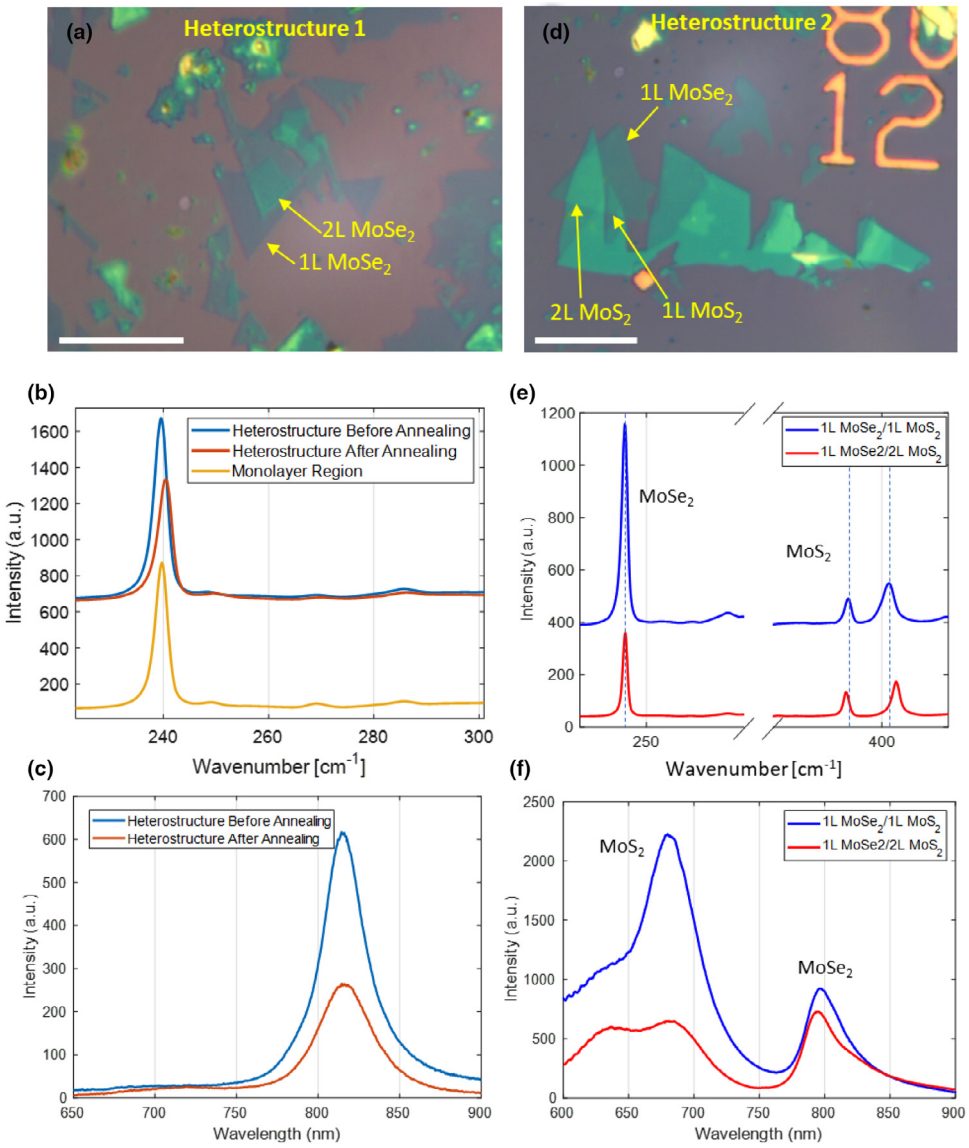

FIGURE 5

(a) Optical image of a bilayer $MoSe_2$ stacked from two pieces of monolayer CVD $MoSe_2$ flakes (Heterostructure 1). (b and c) Raman and PL spectra on Heterostructure 1. Annealing after the transfer improved interlayer contact, which was detected as a red-shift in the $MoSe_2$ A_{1g} Raman peak. PL exhibited a quenching behavior after annealing. (d) Optical image of a heterostructure stacked from a mechanically exfoliated MoS_2 and a CVD grown $MoSe_2$. (e and f) Raman and PL spectra on 1L $MoSe_2$/1L MoS_2 and 1L $MoSe_2$/2L MoS_2 regions, respectively. $MoSe_2$ and MoS_2 components of the heterostructure retained their own electronic structure after the assembly and could be distinguished by spectroscopy. All scale bars: 25 μm.

in both cases despite some minor PL quenching. By contrast, in the 1L $MoSe_2$/2L MoS_2 region, suppression of the MoS_2 PL peak was observed. This is in good agreement with previous reports that a monolayer emits the strongest PL signal compared with bilayers and bulk crystals [59]. Thus, one can infer that the band structures of different materials are preserved as they are assembled into heterostructures and the process of annealing quenches PL signatures due to improved charge transfer. Based on the reported 2D heterostructures in different configurations, we are confident the assembly process applies for structures with subsequent stacking of more layers by repeating the same procedure. We note that the 1L-$MoSe_2$ in Fig. 5a is the flake before water transfer at 75 °C, while the 2L-$MoSe_2$ is the flake after water transfer at 75 °C. A comparison of their corresponding Raman signals shows that there is no significant change in the 2D flakes before and after the water transfer at 75 °C.

Fig. 6 presents further characterization on Heterostructure 2 employing confocal Raman spectroscopy, AFM topography and conductance mapping. The AFM topography, Fig. 6b, shows that the as-transferred $MoSe_2$ flake retains good geometrical integrity and low surface roughness. However, defects can be observed on the area corresponding to MoS_2. Since the MoS_2 was mechanically exfoliated directly onto the SiO_2 substrate, without any additional process before the $MoSe_2$ transfer, the defects are likely caused by polymer residue left on the MoS_2 flake during the tape exfoliation step. The capacitance map, plotted in Fig. 6c, shows a uniform capacitance over the $MoSe_2$ in relation to the background SiO_2. While the MoS_2 flakes display elevated

Please cite this article in press as: S. Dong et al., Materials Today (2022), https://doi.org/10.1016/j.mattod.2022.01.002

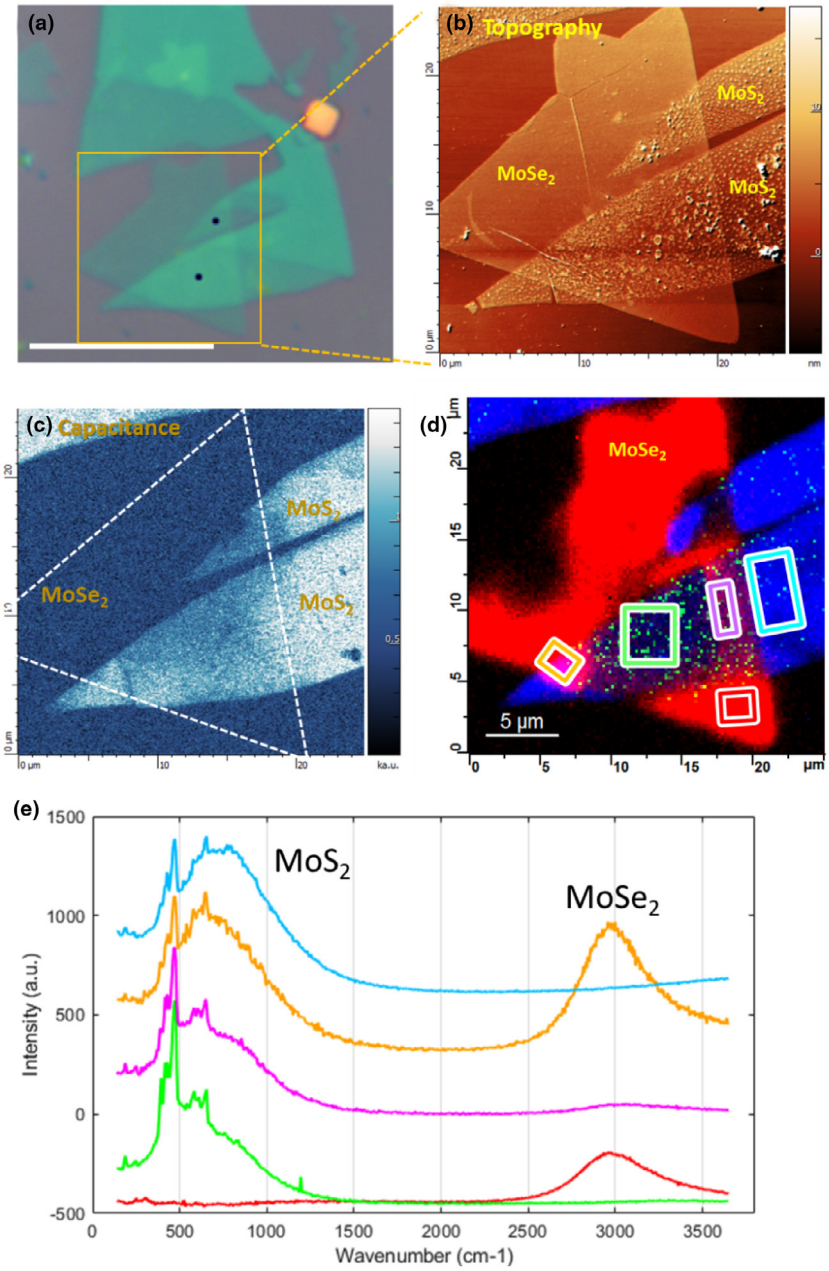

FIGURE 6

(a) Optical image of Heterostructure 2, same as the one shown in Fig. 5b. (b) AFM topography of a zoomed-in region of Heterostructure 2, revealing details of the stacked 2D materials. Polymer residues and trapped air (manifested as spikes and bubbles) are visible on the transferred flake as a result of the tape mechanical exfoliation process. (c) Capacitance (d^2C/dz^2) mapping obtained using scanning capacitance AFM. (d) Combined confocal Raman map of the region of interest on Heterostructure 2 showing the distribution of the intensity of the $MoSe_2$ PL peak at 790 nm (red), MoS_2 PL peak at 660 nm (blue) and the resonant Raman peak of MoS2 at around 465 cm^{-1} (green). (e) Average spectra recorded at different sites of Heterostructure 2. The colors of the curves correspond to locations indicated by colored boxes in d. Note that Si Raman signal has been subtracted from the raw signal to avoid confusions and spectra were offset vertically for clarity.

capacitance. It is worth noting that capacitance uniformity remains high on the region of interest, which is an advantage from a device design perspective. The confocal Raman mapping, however, exhibits more non-uniformity (Fig. 6d). As shown above, for larger spot size Raman measurement, monolayer MoS_2 and $MoSe_2$ independently reflect strong, characteristic Raman signals consistent with the heterostructure. However, the confocal Raman mapping reveals variation across the heterostructures. Fig. 6e contains average Raman signals for differently colored sampling boxes drawn in Fig. 6d. Interestingly, within the $MoSe_2/MoS_2$ heterostructure, there are areas with strong $MoSe_2$ signatures while other areas display no $MoSe_2$ peaks. Such finding provides important information on heterostructure creation and emphasizes the need for characterization of vertically assembled 2D heterostructure with high spatial resolution. We ascribe the heterogeneity to defects and

Please cite this article in press as: S. Dong et al., Materials Today (2022), https://doi.org/10.1016/j.mattod.2022.01.002

intrinsic variation of the material interface from the mechanical exfoliation that produces the bottom MoS_2. Furthermore, these measurements enable identification of regions that can be used for devices of different charge transfer or phonon transport behaviors in 2D heterostructures.

Tip-Enhanced Raman Spectroscopy (TERS) was used to carry out detailed analysis of the 2D material heterostructure assembly with sub-micron spatial resolution. Specifically, we investigated the quality of the interface in the stacked $MoSe_2/MoS_2$, Heterostructure 2 in Fig. 5. At a locally wrinkled site on the $MoSe_2$ flake, an enhanced photoluminescence peak was identified and compared to the surrounding flat region (Fig. 7b). The difference in spectra is in agreement with the interpretation that wrinkles locally introduce funneling of defects and excitons [60,61]. TERS/TEPL maps were acquired with 638 nm laser on different locations to reveal detailed characteristics not available using conventional Raman/PL. Variations in PL were measured at five different areas, indicated by colored boxes in the AFM topography image (Fig. 7a). Each curve shown in Fig. 7b–e is the spectra averaged over the correspondingly colored box area. As expected, distinct MoS_2 PL responses can be found in both the blue and cyan boxes. The PL response in the cyan area is significantly higher, which may be due to the different strain states of the two MoS_2 regions caused by the transfer process. With 785 nm laser, only $MoSe_2$ Raman bands were distinguished on areas with $MoSe_2/MoS_2$, which is not unexpected as this excitation wavelength is in resonance with this material [62]. Rather surprisingly, a higher intensity of the $MoSe_2$ A′(Γ) band was observed over the heterostructure compared to area with only monolayer $MoSe_2$ (Fig. 7c), indicating an enhancing effect on the Raman resonance by the interlayer interaction. By employing the so-called Nano-"Squeegee" process [63], proven to effectively enhance 2D material interfaces using AFM tip wiping, an attempt to further improve the stacked 2D heterostructure inter-

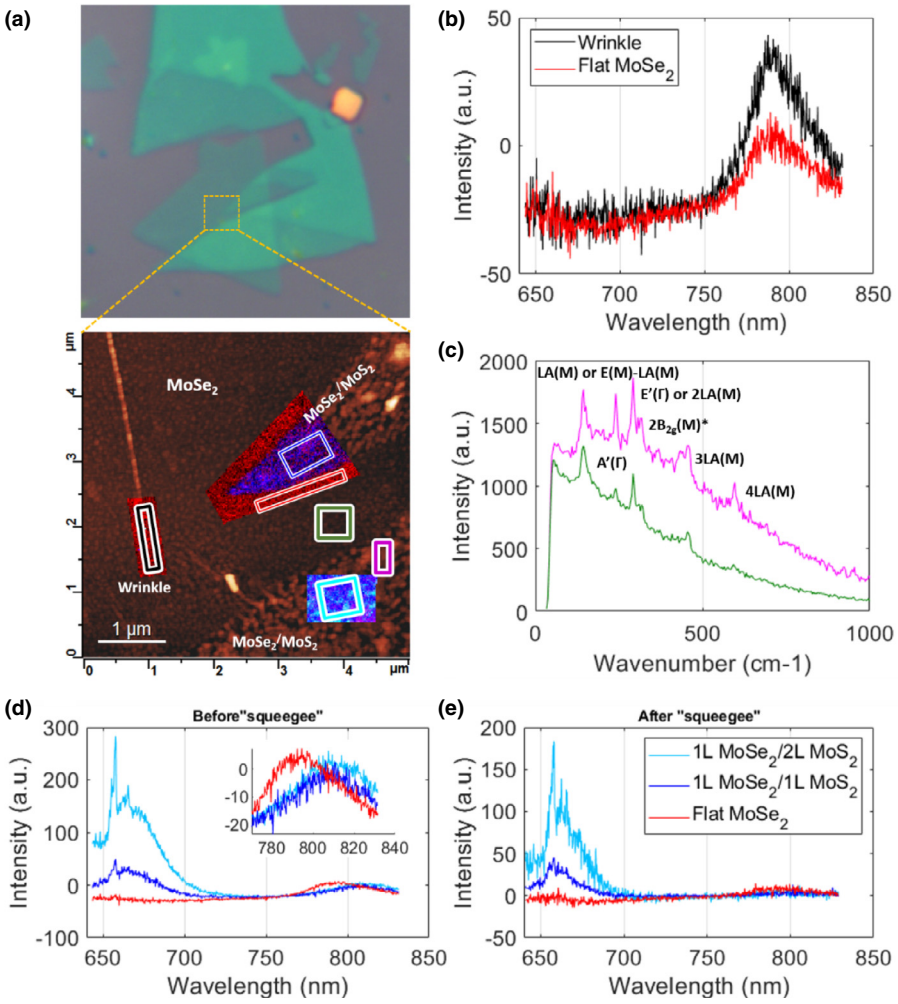

FIGURE 7

(a) AFM topography image of an area on Heterostructure 2 corresponding to a small region of interest as annotated in the optical image. Box labeling colors on the AFM image correspond to averaged TERS plotted signals in other plots. (b) Enhanced photoluminescence was identified on wrinkled MoSe2 compared to flat MoSe2, as expected. (c) TERS signal obtained with 785 nm laser averaged over the purple box on stacked $MoSe_2/MoS_2$ heterostructure and on $MoSe_2$, respectively. (d and e) TERS measurements (638 nm excitation) before and after Nano-"Squeegee" process in boxed areas. The TERS response did not change appreciably after the process. Zoomed insert in d highlights the shift in MoSe2 PL peak positions in vertical heterolayers as compared to the MoSe2 monolayer. Reduced MoSe2 peaks can be attributed to damage from direct interaction with the AFM tip during aggressive squeegee, possibly at the "weak" regions where bubbles/defects exist in the bottom exfoliated MoS_2 flakes.

Please cite this article in press as: S. Dong et al., Materials Today (2022), https://doi.org/10.1016/j.mattod.2022.01.002

face was carried out [63]. The measurements revealed that the "squeegee" process did not significantly change the PL response of the heterostructure (Fig. 7d and e). This indicates that the protocol reported in this paper provides fairly robust interfaces, which are difficult to improve even by very aggressive AFM "squeegee." It is worth noting that the Raman/PL response of these heterostructures are fairly non-uniform down to the sub-micron level, as shown in the color map in Fig. 6d, making it more difficult to define a uniform interface. Such non-uniformity may be caused by the variation of intermolecular potentials and the mismatch of lattice structures.

Concluding remarks

The rapid growth of novel 2D materials demands methods for making monolayer and few-layer structures with fine control of spatial positioning and layer number. In this regard, the reported transfer method represents a novel and simple method for the direct, deterministic transfer, and assembly of 2D materials. The method is based on the competition between water-driven penetration in hydrophilic-hydrophobic interfaces, without the need of sacrificial layers or chemical processes. More importantly, a setup enabling versatile fabrication of 2D heterostructures, of varying lateral and vertical configurations, was demonstrated. The setup achieved highly selective sub-micron level spatial positioning and high rotational accuracy. The simplicity and versatility of the method was demonstrated by transferring exfoliated and CVD grown MoS_2 and $MoSe_2$ in monolayer and heterostructure forms. By employing optical, HRTEM, Raman, and photoluminescence spectroscopy, the high quality of the transferred monolayers and heterostructures was ascertained before and after an annealing step. AFM, confocal Raman, and TERS characterization enabled sub-micron inspection of assembled interfaces and revealed local variations of optical response. By employing these signatures, areas for the fabrication of micro and nanodevices can be identified. Such devices can be fabricated to probe and engineer energy transfer between 2D heterostructures, with the tunability offered by specifically controlled stacking angle and positioning. Furthermore, when combined with developments in lateral 2D heterostructures and 2D dielectrics, we envision exploration of novel device configurations for nano-circuitry and quantum confinement strategies realized by pure 2D material devices stacked to 3D. As such we anticipate adoption of the transfer and characterization methods here discussed in the fabrication of devices based on 2D materials (e.g., TMDCs and MXenes) targeting investigations ranging from electronics, batteries, solar cells, and twistronics devices.

Materials and methods

Materials

Exfoliated MoS_2 flakes were obtained from bulk MoS_2 crystals that were purchased from SPI Supplies, PA, USA. CVD grown $MoSe_2$ was synthesized in Rice University using the method introduced in Ref. 20. PDMS films used to demonstrate the technique were Gel-film products purchased from Gel-Pak, CA, USA. PDMS stamps with protrusions were made from SYLGARD™ 184 Silicone Elastomer Kit from Dow, MI, USA using an SU-8 mold made on a silicon wafer.

Raman and photoluminescence spectroscopy

Analysis of the single- and few-layer TMDC flakes using Raman spectroscopy was carried out with a HORIBA LabRam HR800 system using a 532 nm laser line and an Andor DU970N-FI-328 Peltier cooled CCD detector. The spectral resolution of the system is <1 cm^{-1} and the peak locations were identified by fitting the spectra to a multi-peak Lorentzian line shape. The Raman peak of a silicon wafer at 520 cm^{-1} was used as a reference to calibrate the detector.

High-resolution transmission electron microscopy

The high-resolution transmission electron microscopy (HRTEM) characterization was conducted with the chromatic aberration-corrected TEM (FEI Titan 80-300 ST with an aberration corrector for both the spherical and chromatic correction) at 200 kV acceleration voltage. The images were taken with spherical and chromatic aberration corrected such that $C_s < 5$ μm, and $C_c < 5$ μm.

Experimental setup

Setup for achieving controlled, deterministic transfer was established on a Probe station (need to check model next time with access to labs). A 3-axis manual stage is mounted on the side of the probe station, which controls positions of the glass slide carrying the PDMS transfer stamp. A custom hot plate was built on top of the sample carrying stage of the probe station for heating control during the transfer procedure. The thin hot plate is assembled surrounding a silicone rubber heater (SRFRA-3/10) and a CN7223 Temp/Process controller, both from Omega Engineering, Inc., CT, USA.

Chemical vapor deposition

$MoSe_2$ was grown by CVD method using MoO_3 and Se powder as precursors, and SiO_2/Si as substrate. A crucible containing MoO_3 powder and SiO_2/Si was placed in the center of the furnace. Another crucible containing Se powder was placed near the edge of the furnace. The furnace was heated to 750 °C in 15 min and maintained for another 15 mins before cooling down naturally. H_2/Ar (15% H_2) gas was kept flowing during the entire growth.

AFM, confocal and TERS method

AFM topography and TERS characterization were carried out in air on an OmegaScope-R system (Horiba Scientific), coupled to XploRA confocal Raman spectrometer (Horiba Scientific). A gold-coated OMNI-TERS-SNC probe was used to obtain TERS maps. 638 nm or 785 nm lasers were focused onto the apex of the TERS probe using a ×100, 0.7NA air objective (Mitutoyo). A dedicated TERS imaging mode (SpecTop™) was employed for fast and efficient TERS mapping.

CRediT authorship contribution statement

Siyan Dong: Conceptualization, Methodology, Formal analysis, Investigation, Writing – original draft, Writing – review & editing, Visualization. **Xiang Zhang:** Methodology, Investigation, Writing – review & editing. **S. Shiva. P. Nathamgari:** Methodology, Writing – review & editing. **Andrey Krayev:** Methodology, Formal analysis, Investigation, Writing – review

Please cite this article in press as: S. Dong et al., Materials Today (2022), https://doi.org/10.1016/j.mattod.2022.01.002

& editing, Visualization. **Xu Zhang:** Methodology, Formal analysis, Investigation, Writing – review & editing, Visualization. **Jin Wook Hwang:** Methodology, Formal analysis, Investigation, Writing – review & editing, Visualization. **Pulickel M. Ajayan:** Methodology, Resources, Writing – review & editing, Supervision, Project administration, Funding acquisition. **Horacio D. Espinosa:** Conceptualization, Methodology, Resources, Writing – review & editing, Supervision, Project administration, Funding acquisition.

Declaration of Competing Interest

The authors declare the following financial interests/personal relationships which may be considered as potential competing interests: Dr. Andrey Krayev works for Horiba Scientific.

Acknowledgement

H.D.E. acknowledges support from Army Research Office (ARO) through grant no. W911NF1510068. The authors would like to thank Dr. Chakrapani Varanasi from ARO for supporting the research program and for valuable suggestions. The authors acknowledge support from the Center for Nanoscale Materials (CNM, Argonne National Lab), an Office of Science user facility, supported by the U.S. Department of Energy, Office of Science, Office of Basic Energy Sciences, under Contract No. DE-AC02-06CH11357. This work made use of the NUFAB facility of Northwestern University's NUANCE Center, which has received support from the SHyNE Resource (NSF ECCS-2025633), the IIN, and Northwestern's MRSEC program (NSF DMR-1720139). The authors thank Jianguo Wen for acquiring the HRTEM images and Michael Moody for kind support on the sample annealing process. S.D. thanks Nicolaie Moldovan for his guidance on fabrication processes. S.D. acknowledges the Cabell Terminal Year Fellowship for financial support.

Data Availability

The raw/processed data required to reproduce these findings cannot be shared at this time as the data also forms part of an ongoing study.

References

[1] K.S. Novoselov et al., Science 306 (5696) (2004) 666.
[2] A.H. Castro Neto, K. Novoselov, Rep. Prog. Phys. 74 (2011) 8.
[3] C. Lee et al., Science 321 (5887) (2008) 385.
[4] K.I. Bolotin et al., Solid State Commun. 146 (9–10) (2008) 351.
[5] K.F. Mak et al., Phys. Rev. Lett. 105 (2010) 13.
[6] K.A.N. Duerloo et al., J. Phys. Chem. Lett. 3 (19) (2012) 2871.
[7] D. Lembke, A. Kis, ACS Nano 6 (11) (2012) 10070.
[8] Z. Yin et al., ACS Nano 6 (1) (2012) 74.
[9] B. Radisavljevic et al., Nat. Nanotechnol. 6 (3) (2011) 147.
[10] Y. Shao et al., Electroanalysis 22 (10) (2010) 1027.
[11] S.S.P. Nathamgari et al., Exp. Mech. 59 (3) (2019) 349.
[12] S.S.P. Nathamgari et al., Nano Lett. 19 (6) (2019) 4052.
[13] Y. Liu et al., ACS Appl. Mater. Interfaces 9 (41) (2017) 36137.
[14] J. Pei et al., Adv. Mater. 31 (2) (2019) 1706945.
[15] K. Khan et al., J. Mater. Chem. C 8 (2) (2020) 387.
[16] Z. Huang et al., 2D Materials 2 (3) (2015) 035011.
[17] J.A. Robinsona, APL Mater. 6 (2018) 5.
[18] D. Jariwala et al., ACS Nano 8 (2) (2014) 1102.
[19] Y. Huang et al., ACS Nano 9 (11) (2015) 10612.
[20] Y.J. Gong et al., Adv. Funct. Mater. 26 (12) (2016) 2009.
[21] K.S. Novoselov et al., Science 353 (2016) 6298.
[22] C.R. Dean et al., Nat. Nanotechnol. 5 (10) (2010) 722.
[23] H.Y. Zhu et al., Nat. Nanotechnol. 10 (2) (2015) 151.
[24] X.L. Liang et al., ACS Nano 5 (11) (2011) 9144.
[25] A. Castellanos-Gomez, et al., *2D Mater.* (2014) **1** (1).
[26] Z.X. Lu et al., ACS Nano 10 (5) (2016) 5237.
[27] P.J. Zomer et al., Appl. Phys. Lett. 99 (2011) 23.
[28] T. Uwanno, et al., *2D Mater.* (2015) **2** (4).
[29] X.D. Chen et al., Carbon 56 (2013) 271.
[30] H.V. Ngoc et al., Sci Rep-Uk (2016) 6.
[31] X.Z. Ma et al., Nano Lett. 17 (11) (2017) 6961.
[32] Y. Hou et al., ACS Appl. Mater. Interfaces 12 (36) (2020) 40958.
[33] J.H. Kim et al., Sci Rep-Uk (2019) 9.
[34] G. Jin et al., Sci. Adv. 5 (2019) 7.
[35] C. Yoo et al., ACS Appl. Mater. Interfaces 12 (22) (2020) 25200.
[36] A. Gurarslan et al., ACS Nano 8 (11) (2014) 11522.
[37] H. Li et al., ACS Nano 8 (7) (2014) 6563.
[38] S.S. Han et al., Nano Lett. 20 (5) (2020) 3925.
[39] K. Kang et al., Nature 550 (7675) (2017) 229.
[40] A. Zobel et al., J. Mater. Chem. C 4 (47) (2016) 11081.
[41] S. Wang, G. Wang, G. Peng, Z. Li, Controllable growth of bilayer MoS_2 crystals by reverse-flow chemical vapor deposition, Presented at Earth and Environmental Science, Guangzhou, China, 2020.
[42] J.H. Lee et al., Curr. Appl. Phys. 20 (10) (2020) 1190.
[43] Y. Cao et al., Nature 556 (7699) (2018) 43.
[44] T. Kitabatake, Transfer Process and Transfer Sheet for Use Therein, Dai Nippon Printing Co Ltd, USA, 1979.
[45] R.G. Frieser, J. Electrochem. Soc. 121 (5) (1974) 669.
[46] A. Kozbial et al., Langmuir 31 (30) (2015) 8429.
[47] S. Khodaparast et al., Phys. Rev. Lett. 121 (2018) 26.
[48] S.K. Deng et al., ACS Appl. Mater. Interfaces 9 (8) (2017) 7812.
[49] C.D. van Engers et al., Nano Lett. 17 (6) (2017) 3815.
[50] H. Rokni, W. Lu, Nat. Commun. 11 (1) (2020) 1.
[51] N.N. Mao et al., Small 9 (8) (2013) 1312.
[52] S. Desai et al., J. Nanoeng. Nanomanuf. 4 (3) (2014) 237.
[53] P. Tonndorf et al., Opt. Express 21 (4) (2013) 4908.
[54] A. Jain et al., Nanotechnology 29 (2018) 26.
[55] R. Frisenda et al., Chem. Soc. Rev. 47 (1) (2018) 53.
[56] S. Tongay et al., Nano Lett. 12 (11) (2012) 5576.
[57] X.P. Hong et al., Nat. Nanotechnol. 9 (9) (2014) 682.
[58] H. Li et al., Adv. Funct. Mater. 22 (7) (2012) 1385.
[59] A. Splendiani et al., Nano Lett. 10 (4) (2010) 1271.
[60] C. Cong et al., Adv. Opt. Mater. 6 (2017) 1.
[61] A. Krayev, On the Nature of Increased TERS/TEPL Signal in Wrinkles of 2D Materials (Conference Presentation), SPIE, 2018.
[62] P. Soubelet et al., Phys. Rev. B 93 (15) (2016) 155407.
[63] M.R. Rosenberger et al., ACS Appl. Mater. Interfaces 10 (12) (2018) 10379.

Please cite this article in press as: S. Dong et al., Materials Today (2022), https://doi.org/10.1016/j.mattod.2022.01.002